Nonuniform Radiation Modeling of a Corrugated Plate Photocatalytic Reactor

Huilan Shang
School of Engineering, Laurentian University, Sudbury, ON, Canada P3E 2C6

Zisheng Zhang
Dept. of Chemical Engineering, University of Ottawa, Ottawa, ON, Canada K1N 6N5

William A. Anderson
Dept. of Chemical Engineering, University of Waterloo, Waterloo, ON, Canada N2L 3G1

DOI 10.1002/aic.10440
Published online May 2, 2005 in Wiley InterScience (www.interscience.wiley.com).

Corrugated plate photocatalytic reactors provide a promising photoreactor design due to its potential in enhancing energy efficiency. A detailed model of such reactors is needed for engineering applications and process design. The model for the light absorption in a corrugated plate reactor using a nonuniform radiation source is developed based on first principles. The local area-specific rate of energy absorption (LASREA) distribution on the corrugated plates is examined via simulation. The effect of the design parameters on LASREA is investigated. The results from this research provide feasible basis for design and optimization of corrugated plate photoreactors. © 2005 American Institute of Chemical Engineers *AIChE J,* 51: 2024–2033, 2005
Keywords: modeling, light radiation, photoreactor, photocatalysis

Introduction

Photochemical processes have interested researchers in the last two decades. Active research has been focused on photocatalytic reactions and the potential applications (for example, soil remediation, water treatment, biological decolorization, biodegradation and so on).[1–9] Growing research in the field has lead to a better understanding of catalysts, photocatalysis mechanism as well as reaction kinetics and conditions.[10–14] Research efforts on the related engineering issues, however, have been limited.

Modeling of photocatalytic reactors is essential for successful exploitation, design and scaleup of photocatalytic systems. Radiation fields in photoreactors have been modeled in some literature.[15–19] Radiative transfer in absorbing, reacting, and scattering reaction media has been properly described by a set of integral-differential equations.[20] The radiation fields in (pseudo)homogeneous photoreactors have been described using the local volumetric rate of energy absorption (LVREA) and modeled with the Lambert-Beer's law,[21] and the principles of geometric optics.[22] However, the LVREA is not appropriate for describing the radiation absorption profiles on immobilized catalyst films. In the recent work, modeling of a thin-film slurry photocatalytic reactor has been reported.[23]

Zhang et al.[24] investigated the recapture of reflected photons on the radiation absorption of an immobilized catalyst film in a corrugated plated reactor and found that corrugated plate can enhance the energy absorption efficiency significantly. Local area-specific rate of energy absorption (LASREA) was used to express the radiation absorption profiles in heterogeneous photoreactors. The main shortcoming of the previous work was that the geometry and spacing of the energy source (fluorescent lamps and the solar UV) were not incorporated with the assumption that the incidence rays on the reactor cover (lamp sleeve) were uniform. Thus, the resulting model equations fail to account for UV variations in the longitudinal direction. In

Correspondence concerning this article should be addressed to H. Shang at hshang@laurentian.ca.

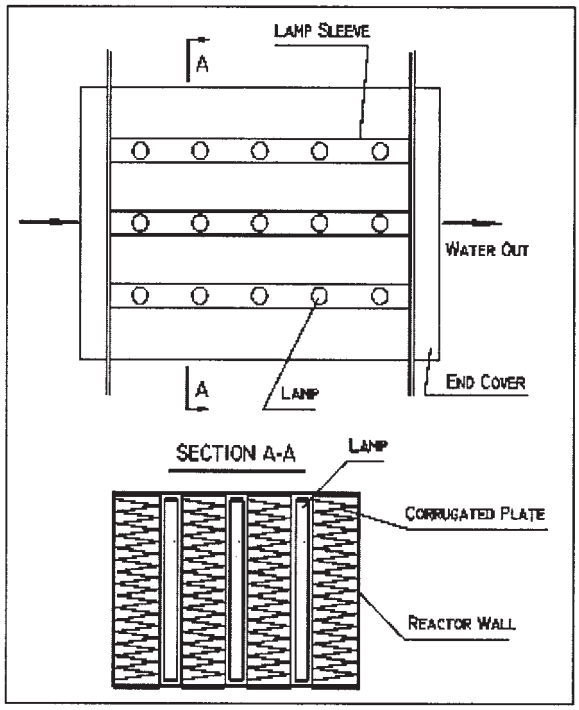

Figure 1. Corrugated-plate reactor: top view and cross-sectional view.

practical applications, nonuniform radiation on sleeves often occurs due to discontinuous distribution of the UV lamps.

In this article, a new model for the light absorption of the immobilized catalyst film, TiO_2 film, in a corrugated plated reactor is developed by incorporating the cylindrical geometry of the fluorescent lamps. The newly developed model represents the more rigorous and accurate description of the light refraction and absorption in a corrugated plate reactors, and can account for the longitudinal UV variation of the lamps. The light absorption distribution on the reactor plates is examined via simulation, and the effects of the design parameters on the light absorption distribution are investigated. The resulting model equations and approaches can provide effective references for the design of corrugated plated reactors. The results in this article can be directly used for the optimization and scaleup of corrugated plate photocatalytic reactors according to user specifications.

Equipment and Materials

In this article, a lamp-illuminated corrugated plate photocatalytic reactor is considered, as in Figure 1. Catalyst is immobilized on both sides of the corrugated plates. For the purpose of modeling, a single corrugation and a single lamp are taken from Figure 1, and placed under a rectangular coordinate system, as shown in Figure 2 for uniform radiation and Figure 3 for nonuniform radiation. The height and length of the corrugated plate, B and L, are kept constant at 0.05 m and 0.8 m during the simulation. The effect of the corrugation angle is examined numerically. The lamp sleeve examined is a UV transmitting Plexiglas (G-UVT) sheet with thickness of 6.35 mm. The radiation sources considered are UV cylindrical fluorescent lamps.

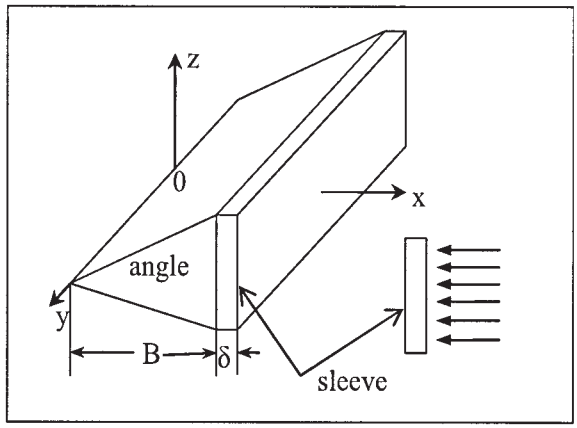

Figure 2. Coordinate system for a uniform radiation corrugated plate.

Uniform Radiation Modeling

In the previous work, UV absorption was modeled for both solar radiation and lamp radiation assuming uniform radiation pattern on the outer surface of the sleeves.[24] Figure 2 shows the coordinate system used in modeling and the radiation pattern on the outer surface of the sleeves. For obtaining the UV absorption from the lamp radiation, the spectral local area-specific rate of energy incidence on corrugated plate was modeled, followed by absorption and reflection of the incidence energy on TiO_2 films. The process was iterated until the reflected energy became negligible. The total UV absorption at each point of the plates was obtained from summation of the energy absorption of the incident energy, as well as the reflected energy with different times of reflection between the upper and lower wings of the corrugated plate.

On the basis of the coordinate system in Figure 2, the spectral local area-specific rate of energy incidence on any point of the upper wing of the corrugated plate $P'(x', y', z')$, due to radiation from the lamp sleeve, was obtained as follows

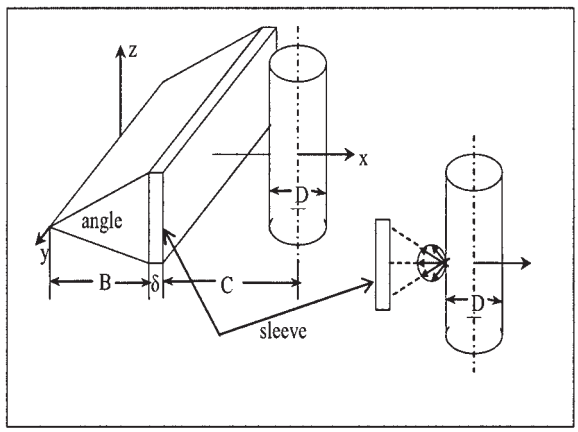

Figure 3. Coordinate system for a nonuniform radiation corrugated plate.

$$I_u^s(y', z') = \frac{W_\lambda}{\pi}\left(\frac{n_w}{n_a}\right)^2 \int\int_{S1} \frac{\cos\psi_1}{d_1^2}\cos\psi_w \times \exp(-k_3\delta[1-(n_w/n_s\sin\psi_w)^2]^{-0.5} - k_4 d_1)dydz \quad (1)$$

where surface $S1$ represents the region on the lamp sleeve that illuminates point $P'(x', y', z')$ of the upper wing. The relation between the incident and the absorbed energy at wavelength λ can be expressed as

$$q_u^s(y', z') = a(\lambda)I_u^s(y', z') \quad (2)$$

where $a(\lambda)$ indicates the dimensionless absorption coefficient of the catalyst film as a function of photon wavelength.

Using the symmetry of the upper and lower wings of the corrugated plate, the spectral local area-specific rate of energy incidence on the upper wing point $P'(x', y', z')$ due to the first reflection from the lower wing was obtained as

$$I_u^{(1)}(y', z') = \frac{1-a(\lambda)}{\pi}\int\int_l \frac{I_u^s(y', -z')\cos\psi_4\cos\psi_5}{d_2^2} \times \exp(-k_4 d_2)dydz \quad (3)$$

where d_1 indicates the distance between a point $P'(x', y', z')$ on the upper wing and a point $P(x, y, z)$ on the lamp sleeve, d_2 indicates the distance between a point $P'(x', y', z')$ on the upper wing, and a point $P''(x'', y'', z'')$ on the lower wing, ψ_1 is the angle between the normal of the upper wing and line PP', ψ_4 is the angle between the normal of the lower wing, and line $P''P'$, ψ_5 is the angle between the normal of the upper wing and line $P''P'$. These parameters can be calculated using the following equations

$$d_1^2 = (z'\cot\alpha - B)^2 + (y' - y)^2 + (z' - z)^2 \quad (4)$$

$$d_2^2 = (\cot(z' + z))^2 + (y' - y)^2 + (z' - z)^2 \quad (5)$$

$$\cos\psi_1 = \sin\alpha(B - z\cot\alpha)/d_1 \quad (6)$$

$$\cos\psi_w = (B - z'\cot\alpha)/d_1 \quad (7)$$

$$\cos\psi_4 = 2z'\cos\alpha/d_2 \quad (8)$$

$$\cos\psi_5 = 2z''\cos\alpha/d_2 \quad (9)$$

Similarly, the energy incidence and absorption from second, third and n^{th} reflection can be determined. This process can be iterated until the reflected energy become very small. Then the total energy absorption at point $P'(x', y', z')$ of the corrugated plate is obtained from the summation of the energy absorption of the incident energy and reflected energy.

The uniform radiation model provides useful relations among the energy from a UV-Lamp and the incidence energy on TiO_2 film, as well as the energy absorption and reflection, and can be applied to solar-illuminated systems, as well as lamp illuminated systems when the lamps are densely packed. In practical applications, however, the lamps in a photoreactor are often arranged discontinuously at a desired spacing in the sleeves. This discontinuity inevitably lead to a nonuniform radiation field on the sleeves. Therefore, it is necessary to reexamine the light radiation, incidence and absorption relations based on the discontinuous lamp arrangement.

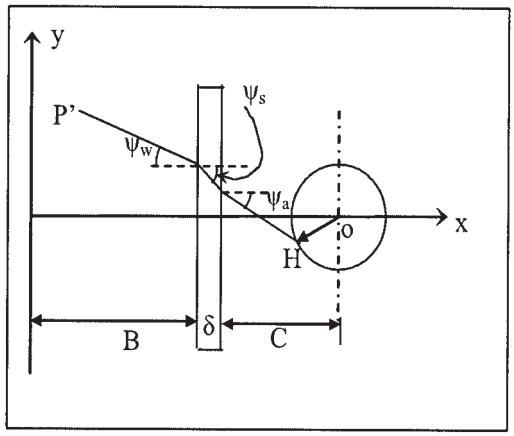

Figure 4. Cross-sectional view of a nonuniform radiation corrugated plate.

Nonuniform Radiation Modeling

In most applications, a uniform lamp radiation field on a lamp sleeve cannot be obtained. In this section, the light incidence and absorption models are developed based on a more realistic radiation source—discontinuously distributed fluorescent lamps. The challenge of modeling the nonuniform lamp radiation lies in formulation of the incidence energy from a cylindrical lamp to corrugated plates. As long as the incidence energy from the lamp is formulated, absorption and reflection of the UV-ray between two conjugate wings of the corrugated plate can be determined in the same way as for uniform radiation, discussed in the last section. Therefore, nonuniform radiation modeling in this section focuses on the incidence energy from the lamps to the corrugated plate wings. For the purpose of simplicity, only one lamp is considered. The effect of an array of lamps can be inferred from superimposition of the effect of single lamps.

For the convenience of formulation, a coordinate system, as in Figure 3, is used on a corrugated plate and a lamp. Figure 4 gives a cross-sectional view of the corrugated plate, the lamp and the coordinate system. The incidence energy at any point of the corrugated plate can be obtained from summation of the energy irradiated from each point of the lamp surface. Due to symmetry of the upper wing and the lower wing of the plate, it is adequate to model the incidence energy for any point on the upper wing and the models for the lower wing can be easily inferred.

Let $P'(x', y', z')$ indicate a point on the upper wing of the corrugated plate, $H(x_H, y_H, z_H)$ be a point on the surface of the fluorescent lamp, ξ be the angle between OH and X-axis ($\xi \in [-\pi, \pi]$). The coordinate of point H can also be expressed as

$$x_H = B + C + \delta - \frac{D}{2}\cos\xi$$

$$y_H = \frac{D}{2}\sin\xi, \tag{10}$$

where B is the height of the corrugated plate, C is the distance between the outer surface of the lamp sleeve and the central axis of the lamp, D is the diameter of the lamp, and δ is the thickness of the lamp sleeve.

To determine the area-specific incidence energy at point P′ due to the radiation from point H, it is necessary to have the geometric path of the light ray from H to P′. The incidence angle ψ_a at which the light ray from point H on the lamp falls on the lamp sleeve, and the refraction angles in penetrating the air/solid and solid/liquid interfaces, ψ_s and ψ_w, can be derived using the principles of geometric optics. The following equation gives an implicit formula for the refraction angle ψ_w

$$(B - z'\cot\alpha)\frac{\sin\psi_w}{\sqrt{1-\sin^2\psi_w}} + \delta\frac{\frac{n_w}{n_s}\sin\psi_w}{\sqrt{1-\frac{n_w^2}{n_s^2}\sin^2\psi_w}} + (x_H - B - \delta)\frac{\frac{n_w}{n_a}\sin\psi_w}{\sqrt{1-\frac{n_w^2}{n_a^2}\sin^2\psi_w}} = \sqrt{(y'-y_H)^2+(z'-z_H)^2}, \tag{11}$$

where α is the half angle of the corrugated plate, n_w, n_s and n_a are the refractive indices of reaction media (mostly water), the Plexiglas lamp sleeve and the air, respectively. Detailed derivation of Eq. 11 is provided in the Appendix. This equation can be solved using numerical Newton's method with $\sin\psi_w$ being the unknown. With the derived refraction angle ψ_w, the refraction angle in the solid phase ψ_s, and the incidence angle in the air phase ψ_a can be obtained by directly applying Snell's Law

$$\sin\psi_s = \frac{n_w}{n_s}\sin\psi_w$$

$$\sin\psi_a = \frac{n_w}{n_a}\sin\psi_w \tag{12}$$

In the path of the light ray from H to P′, let the light ray intercepts the outer surface of the lamp sleeve at point G and intercepts the inner surface of the sleeve at point P. The relation for cosine of the angle between the normal of the upper wing and line PP′ can be developed as

$$\cos\psi_1 = \frac{d_s\tan\alpha - (z_H - z')\tan\psi_w}{d_s}\cos\psi_w\cos\alpha \tag{13}$$

while the angle between the normal of the lamp at point H and line GH can be written as

$$\cos\psi_2 = \frac{2\cos\psi_a(x_H - B - C - \delta)}{D} + \frac{2y_H\sin\psi_a(y_H - y')}{Dd_s} \tag{14}$$

where

$$d_s = \sqrt{(y' - y_H)^2 + (z' - z_H)^2} \tag{15}$$

and its geometric meaning can be seen from the detailed development of formula for $\cos\psi_1$ and $\cos\psi_2$. Note that $\cos\psi_1$ for nonuniform radiation in Eq. 13 is much more involved than that for uniform radiation, as described in Eq. 6. The development of Eq. 13 and 14 is provided in the Appendix.

The energy conservation law and the principles of the geometric optics are used to determine the local area-specific rate of energy incidence on any point of the upper wing P′(x', y', z'), due to radiation from the cylindrical lamp. Assuming the diffusive irradiation pattern on the lamp surface, as in Figure 3, the light intensity at point H on the lamp surface per unit area per unit solid angle in the direction of ψ_2 is $W_\lambda/\pi\cos\psi_2$, where W_λ can be calculated from the normal distribution function[24]

$$W_\lambda = \frac{W}{\sqrt{2\pi}\,\sigma}\exp\left(-\frac{(\lambda - 353)^2}{2\sigma^2}\right) \tag{16}$$

and W is the energy intensity of the lamp, W_λ is the spectral energy intensity of the lamp at the wavelength of λ and σ = 15.75 nm.

The energy radiated from an infinite small area dA_1 at point H into a solid angle $\sin\psi_a d\psi_a d\theta$ is

$$dE_l = \frac{W_\lambda}{\pi}\cos\psi_2\sin\psi_a d\psi_a d\theta dA_1 \tag{17}$$

The area of the upper wing that is covered by the light rays from point H within the solid angle $\sin\psi_a d\psi_a d\theta$ of the cylindrical lamp can be derived from analyzing the geometry of the light refraction pattern from the cylindrical lamp to the corrugated plate. Define

$$d_r = \left(\frac{x_H - B - \delta}{\cos^2\psi_a} + \frac{\delta}{\cos^2\psi_s}\frac{n_a\cos\psi_a}{n_s\cos\psi_s} + \frac{B - x'}{\cos^2\psi_w}\frac{n_a\cos\psi_a}{n_w\cos\psi_w}\right)\cos\psi_w \tag{18}$$

The area of the upper wing that is covered by the light rays within the solid angle $\sin\psi_a d\psi_a d\theta$ from the lamp surface can be formulated as

$$dS_w = \frac{d_s d_r}{\cos\psi_1}d\psi_a d\theta \tag{19}$$

The detailed derivation of dS_w is provided in the Appendix.

For the energy leaving dA_1 from point H of the lamp surface at the angle of ψ_2, if there is no energy loss, the fraction

intercepted by dA_2 at point P′ of the upper wing can be written as

$$\frac{dA_2}{dS_w}\,dE_L = \frac{1}{\pi d_s d_r}\,W_\lambda \cos\psi_1 \cos\psi_2 \sin\psi_a\, dA_1 dA_2 \qquad (20)$$

Incorporating the transmittance loss in the acrylic lamp sleeve, the energy received per unit area from the unit area of the lamp at upper wing point P′(x', y', z'), can then be expressed as

$$i = \frac{1}{\pi d_s d_r}\,W_\lambda \cos\psi_1 \cos\psi_2 \cos\psi_a \exp(-k_3\delta/\cos\psi_s) \qquad (21)$$

Therefore, the incidence energy per unit time per unit area at P′(x', y, z') is

$$I_u^s(y', z') = \int\int_{A_1} i\,dA_1 = \frac{D}{2}\int_{z_{Hl}}^{z_{Hu}}\int_{\xi_l}^{\xi_u} i\,d\xi\,dz_H \qquad (22)$$

where z_{Hu}, z_{Hl}, ξ_l and ξ_u represent the upper and lower boundaries of the integration on the surface of the lamp. For integration, the boundaries z_{Hu}, z_{Hl}, ξ_l and ξ_u can be calculated using the geometric relations of the light rays in the boundaries, formulation of which is relatively straightforward and is omitted in the article.

As the area specific incidence energy of the upper (and lower) wing of the corrugated plate is derived, the incidence energy then experiences absorption and reflection, which can be calculated in the same way as for the uniform lamp radiation. The overall light absorption is summation of the light absorption of the incident energy and reflected energy with different times of reflections between the upper and lower wings of the corrugated plate. Although the equations developed in this section apply to corrugated plate photoreactors, some of them can as well be used in photoreactors of different design with slight modifications.

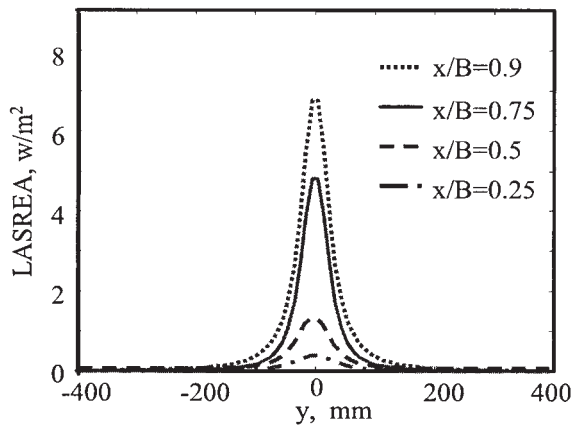

Figure 5. LASREA profile of a lamp-illuminated corrugated plate in water phase (angle = 7°).

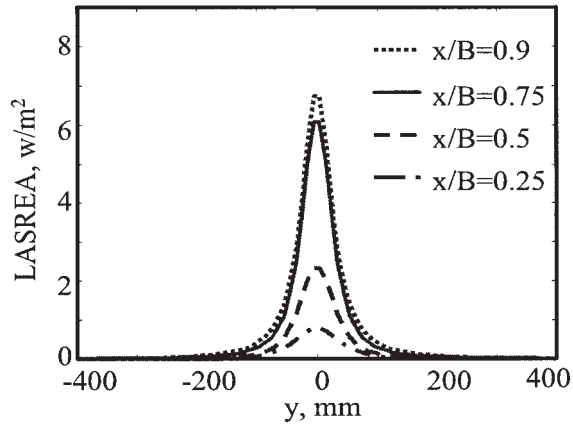

Figure 6. LASREA profile of a lamp-illuminated corrugated plate in water phase (angle = 10°).

Simulation Results

In this section, the area specific energy intensity on a corrugated plate is simulated using the equations developed in the last section. The parameters used in the simulation are: the height of the corrugated plate $B = 0.05$ m, the length of the corrugated plate $L = 0.8$ m, the diameter of the lamp $D = 0.038$ m, the distance of the lamp axis to the outer surface of the lamp sleeve $C = 0.02165$ m, the thickness of the lamp sleeve $\delta = 6.35$ mm, the refractive index of the reaction media $n_w = 1.33$, the refractive index of the lamp sleeve $n_s = 1.49$, the refractive index of the air $n_a = 1.00$, the extinction coefficient of Plexiglas G-UVT $k_3 = 0.2185$, the irradiance intensity of the lamp surface $W = 10{,}000$ W/m^2. In the calculation, wavelength $\lambda = 353$ nm is used, the number of time that the light at $\lambda = 353$ nm is reflected between the upper wing and the lower wing is 13, and the spectral irradiance energy is $W_{353} = 253$ W/m^2.

In the simulation, the LASREA profiles on the TiO_2-coated corrugated plates with various conditions and parameters have been investigated. To compare the energy distribution obtained from the nonuniform radiation model with that from the uniform radiation model, the LASREA profiles in the water phase system, with corrugation angles of 7°, can be examined, as in

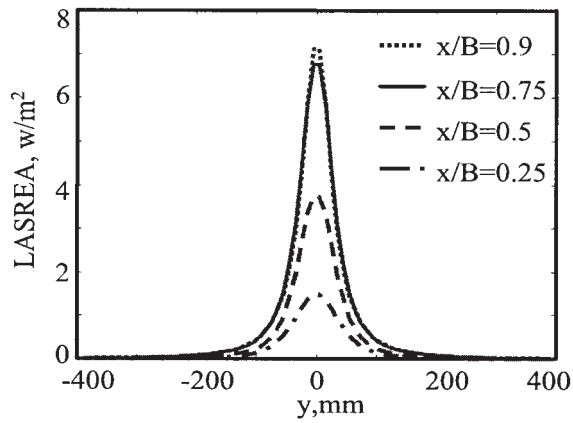

Figure 7. LASREA profile of a lamp-illuminated corrugated plate in water phase (angle = 14°).

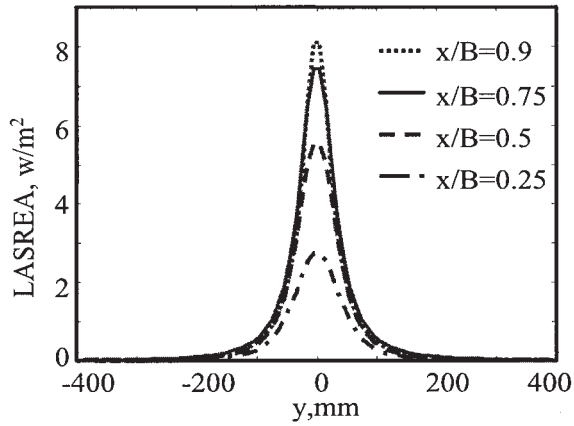

Figure 8. LASREA profile of a lamp-illuminated corrugated plate in water phase (angle = 20°).

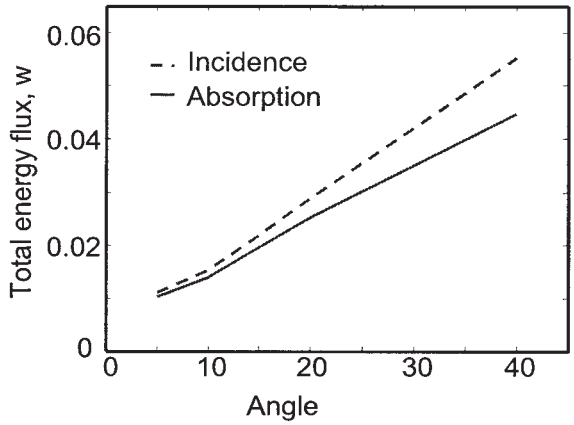

Figure 10. Total incidence energy vs. absorption energy with different corrugation angles.

Figure 5. Note that, in contrast to the uniform radiation model that does not account for the longitudinal variation of the energy intensity, the developed nonuniform radiation model can provide the energy intensity variation in the longitudinal direction (*Y*-axis direction). The obtained energy intensity and distribution in the longitudinal direction (*Y*-axis direction) can provide useful information for lamp spacing design in photoreactors.

The corrugation angle is an important design parameter and its impact on the absorption energy intensity is examined. Figures 5 through 9 show the LASREA profiles on the TiO_2-coated corrugated plates in the water phase systems, with corrugation angles being 7, 10, 14, 20, and 40, respectively. The results indicate that the LASREA increases as the corrugation angle grows, due to the fact that the increased corrugation angle has a larger "window" open to illumination and accommodates UV-rays from a larger area of the lamp surface. It is noted that the radiation field are more uniform in the direction of *X*-axis for a larger corrugation angle. This result can be combined with specific reaction kinetics in determining the proper corrugation angles.

Figure 10 shows the variation of the total energy flux on a single corrugate plate (upper or lower plate) with the corrugation angle. It is observed that the difference between the incidence energy and the absorption energy increases as the corrugation angle increases. The reduced difference between the incidence energy and the absorption energy for smaller corrugation angles indicates that the smaller angle has higher energy efficiency due to the increased number of repeated reflections between upper and lower plates. Since the height and the length of the corrugated plate were kept constant, smaller corrugation angle corresponds to smaller cross-sectional area in the plane of the inner sleeve surface for a single corrugation and more corrugates for a specified reactor size. Therefore, it is reasonable to investigate the impact of corrugation angles on energy efficiency by examining the cross-sectional area-specific energy in the plane of the inner sleeve surface (that is, total energy of a single plate divided by the area of the inner sleeve surface covering the plate). Figure 11 shows that the cross-sectional area-specific energy flux decreases and the energy loss increases as the corrugation angle increases. In contrast to the assumption of the uniform energy distribution in the previous work, Figure 11 also highlights the nonuniform energy distribution on the lamp sleeve.

To investigate the effect of reaction media on the radiation

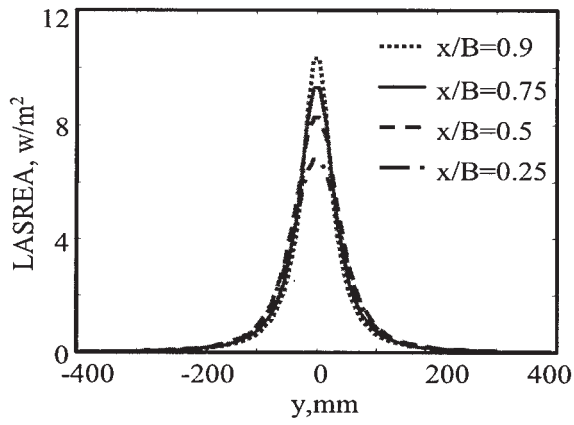

Figure 9. LASREA profile of a lamp-illuminated corrugated plate in water phase (angle = 40°).

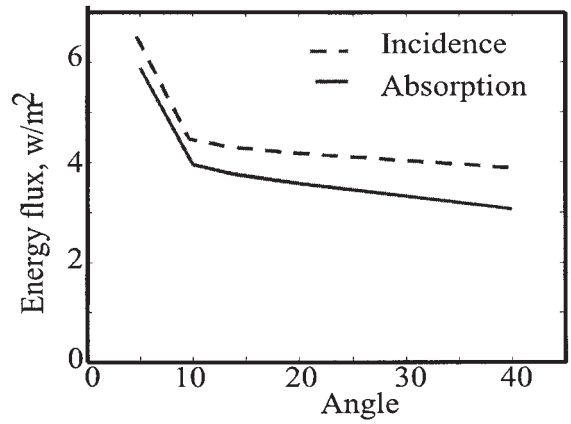

Figure 11. Cross-sectional area-specific incidence energy flux vs. absorption energy flux with different corrugation angles.

field, the LASREA for air phase reaction media is simulated and the result is shown in Figure 12. Comparison of Figure 12 and Figure 6 indicates that water phase generates more uniform LASREA profile in the *X*-axis direction than air phase. It is noticed that air phase has larger absorption energy rate at the sleeve end of the plate while water phase has larger energy intensity for water phase at the "deeper" end of the plate. The radiation field difference for water phase and air phase results from the effect of light refraction from the lamp to the corrugated plate.

The effect of the lamp sleeve on the energy profile was studied by comparing the LASREA profile for a corrugation plate having a lamp sleeve 6.35 mm thick with that having no lamp sleeve. Figure 13 illustrates the LASREA profile for a corrugated plate with no lamp sleeve. In comparison with Figure 6, the corrugation plate with no sleeve leads to the significantly increased LASREA. The reduced energy intensity for the reactor plate with a sleeve 6.35 mm thick results from the significant energy decays in passing the solid sleeve. This implies that thick lamp sleeves are accompanied with significant energy loss and a tradeoff between the desired sleeve strength and the energy loss has to taken into consideration in the reactor design.

Conclusions

The radiation field from a nonuniform energy source is modeled for a TiO_2 filmed corrugated plate photoreactor. In comparison to the existing models, the proposed model realistically incorporates the lamp geometric, diffusive pattern on the surface of the lamp, incidence and refraction of the UV-rays. The results from the developed model can be directly used in the reactor design and scale-up.

On the basis of the developed model equations, simulation was performed to investigate the energy absorption rate on the surface of TiO_2 film in the corrugated plate. The results indicate that a smaller corrugation angle can recapture the reflected photon and result in a high-energy efficiency, but it may generate less uniform absorption rate profile across the corrugation plate from corrugation angle end to the sleeve end. The effect of the reaction media and the sleeve thickness was investigated. It is found that air phase results in less uniform energy rate profile and thin sleeve can significantly reduce the energy loss. The results obtained in this article can be applied to optimize the reactor design, such as the corrugation angle, lamp spacing, the sleeve thickness. The combination of the resulting radiation models with specific reaction kinetics also allows one to study the photoreaction mechanism occurring in a photoreactor.

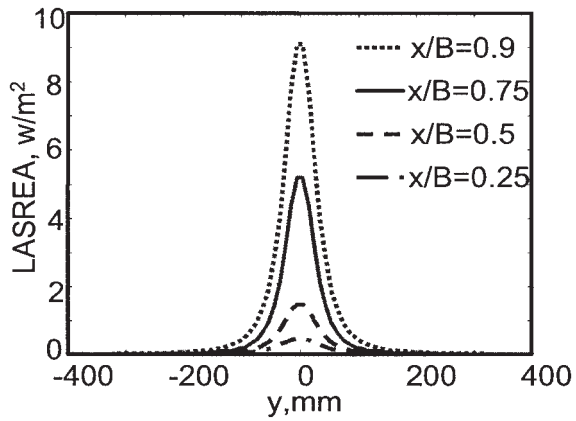

Figure 12. LASREA profile of a lamp-illuminated corrugated plate in air phase (angle = 10°).

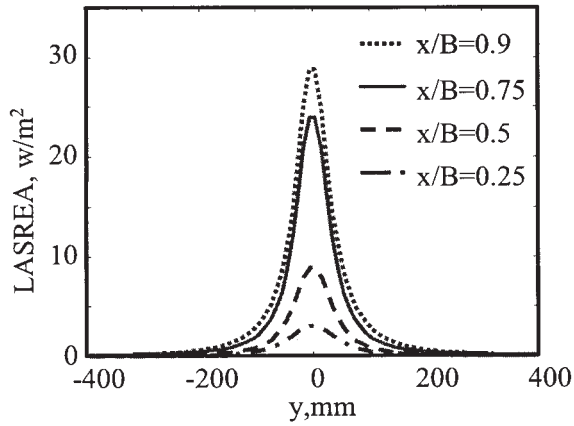

Figure 13. LASREA profile of a lamp-illuminated corrugated plate with no sleeve in water phase (angle = 10°).

Acknowledgments

The financial support from Natural Sciences and Engineering Research Council of Canada is gratefully appreciated.

Notations

$a(\lambda)$ = dimensionless absorption coefficient of the catalyst film as a function of photowavelength
B = height of the corrugated plate
C = distance of the lamp axis to outer surface of the lamp sleeve
D = diameter of the lamp
k_3 = extinction coefficient of Plexiglas G-UVT
n_a = refractive index of the air
n_s = refractive index of the Plexiglas lamp sleeve
n_w = refractive index of the reaction medium (mostly water)
(x', y', z') = rectangular Cartesian coordinate for a point on the upper wing of a corrugated plate
(x, y, z) = rectangular Cartesian coordinate for a point on the inner surface of the lamp sleeve
(x'', y'', z'') = rectangular Cartesian coordinate for a point on the lower wing of a corrugated plate
(x_H, y_H, z_H) = rectangular Cartesian coordinate for a point on the surface of the lamp
W_λ = spectral irradiance energy rate on the surface of the lamp
α = half-angle of the corrugated plate, degrees
δ = thickness of the lamp sleeve
ψ_a = angle of a light ray with respect to the normal of the lamp sleeve at the airs side
ψ_s = angle of a light ray with respect to the normal of the lamp sleeve in the sleeve
ψ_w = angle of a light ray with respect to the normal of the lamp sleeve at the water side
ξ = angular coordinate of a point on the surface of the lamp

Literature Cited

1. Matthews RW. Photooxidation of organic impurities in water using thin films of titanium dioxide. *J Phys Chem.* 1987;91:3328–3333.
2. Aguado MA, Giménez J, Cervera-March S. Continuous photocatalytic

treatment of Cr(VI) effluents with semiconductor powders. *Chem Eng Commun.* 1991;104:71–85.
3. Holden W, Marcellino A, Valic D, Weedon AC. Titanium dioxide mediated photochemical destruction of trichloroethylene vapors in air. *Photocatalytic Purification and Treatment of Water and Air,* Ollis DF, Al-Ekabi H. eds., Elsevier, Amsterdam, 393 (1993).
4. Lawton LA, Robertson PKJ, Jaspars M. Detoxification of microcystins (cyanobacterial hepatotoxins) using TiO_2 photocatalytic oxidation. *Environ Sci Technol.* 1999;33:771–775.
5. Lin WY, Rajeshwar K. Photocatalytic removal of nickel from aqueous solutions using ultraviolet-irradiated TiO_2. *J Electrochem Soc.* 1997; 144:2751–2756.
6. Mehos MS, Turchi CS. Field testing solar photocatalytic detoxification on TCE-contaminated groundwater. *Environ Prog.* 1993;12:194–199.
7. Hong J, Ottaki M. Effects of photocatalysis on biological decolorization reactor and biological activity of isolated photosynthetic bacteria. *J of Biosci and Bioeng.* 2003;96:298–303.
8. Martín CA, Alfano OM, Cassano AE. Decolorization of water for domestic supply employing UV radiation and hydrogen peroxide. *Catalysis Today.* 2000;60:119–127.
9. Bolduc L, Anderson WA. Enhancement of the biodegradability of model wastewater containing recalcitrant and inhibitory chemical compounds by photocatalytic pre-oxidation. *Biodegradation.* 1997;8: 237–249.
10. Sanchez L, Perel J, Domenech X. Aniline degradation by combined photocatalysis and ozonation. *Appl Catal B: Environ.* 1998;19:59–65.
11. Serrano B, Lasa HD. Photocatalytic degradation of water organic pollutants: pollutant reactivity and kinetic modeling. *Chem Eng Sci.* 1999;54:3063–3069.
12. Fujishima A, Rao TN, Tryk DA. Titanium dioxide photocatalysis. *J of Photochem and Photobio, C: Photochemistry Reviews.* 2000;1:1–21.
13. Brandi RJ, Rintoul G, Alfano OM, Cassano AE. Photocatalytic reactors: reaction kinetics in a flat plate solar simulato. *Catalysis Today.* 2002;76:161–175.
14. Jiang Z, Wang H, Huang H, Cao C. Photocatalysis enhancement by electric field: TiO_2 thin film for degradation of dye X-3B. *Chemosphere.* 2004;56:503–508.
15. Alfano OM, Romero RL, Cassano AE. Radiation field modeling in photoreactors—1: homogeneous media; 2. heterogeneous media. *Chem Eng Sci.* 1986;41:421–444, 1137–1153.
16. Romero RL, Alfano OM, Cassano AE. Cylindrical photocatalytic reactors: radiation absorption and scattering effects produced by suspended fine particles in an annular space. *Ind Eng Chem Res.* 1997; 36:3094–3109.
17. Pasquali M, Santarelli F, Porter JF, Yue PL. Radiative transfer in photocatalytic systems. *AIChE J.* 1996;42:532–537.
18. Cabrera MI, Alfano OM, Cassano AE. Novel reactor for photocatalytic kinetic studies. *Ind Eng Chem Res.* 1994;33:3031–3042.
19. Marinangeli RE, Ollis DF. Photo-assisted heterogeneous catalysis with optical fibres: I. isolated single fibre. *AIChE J.* 1977;23:415–426.
20. Cassano AE, Martín CA, Brandi RJ, Alfano OM. Photoreactor analysis and design: fundamentals and applications. *Ind Eng Chem Res.* 1995; 34:2155–2201.
21. Rizzuti L. Absorption of light energy in photoreactors. *Photoelectrochemistry, Photocatalysis, and Photoreactors,* M. Schiavello, ed., D. Reidel Publishing, 1985;587.
22. Roger M, Villermaux J. Modeling of light absorption in photoreactors: part 1. general formulation based on the laws of photometry. *Chem Eng J.* 1979;17:219–226.
23. Puma GL, Yue PL. Modelling and design of thin-film slurry photocatalytic reactors for water purification. *Chem Eng Sci.* 2003;58:2269–2281.
24. Zhang Z, Anderson WA, Moo-Young M. Rigorous modeling of UV absorption by TiO_2 film in a photocatalytic reactor. *AIChE J.* 2000; 46:1461–1470.

Appendix

Calculation of the refraction angle ψ_w

To determine the geometric path of the light rays from lamp surface to the corrugated plate, it is necessary to compute the incidence and the refraction angle of the light ray in crossing the lamp sleeve. Refraction plays an important impact on the light path, and the incidence energy flux from lamp to plate. Let ψ_w be the refraction angle in water phase, ψ_s be the refraction angle in sleeves phase, ψ_a be the incidence angle in air phase. Given point $P'(x', y', z')$ on the upper wing of the corrugated plate and $H(x_H, y_H, z_H)$ on the surface of the lamp, draw a line from P' perpendicular to the sleeve surface until H_0, such that H_0 and H have the same X-coordinates (see Figure A1). The line $P'H_0$ intercepts the inner and outer surfaces of sleeve at P_0 and G_0, respectively. The line from P (the point on the inner surface of sleeve) perpendicular to the sleeve surfaces intercepts with the outer surface of sleeve at point G'. Similarly, the line from G perpendicular to the sleeve surfaces intercept with the line HH_0 at H'.

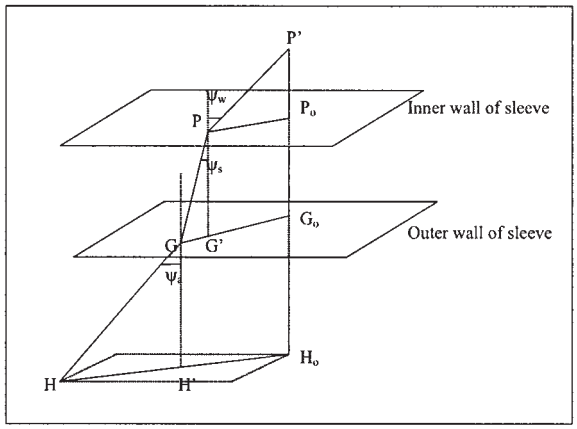

Figure A1. Refraction and the incidence angles.

From Figure A1, it is clear that

$$|HH_0| = |PP_0| + |GG'| + |HH'| \tag{A1}$$

The distance of the lines HH_0, PP_0, GG' and HH' can be obtained from the geometric relations and Snell's law as

$$|HH_0| = d_s = \sqrt{(y' - y_H)^2 + (z' - z_H)^2} \tag{A2}$$

$$|PP_0| = |P'P_0|\tan\psi_w = (B - z'\cot\alpha)\frac{\sin\psi_w}{\sqrt{1 - \sin^2\psi_w}} \tag{A3}$$

$$|GG'| = |PG'|\tan\psi_s = \delta\frac{n_w/n_s\sin\psi_w}{\sqrt{1 - n_w^2/n_s^2\sin^2\psi_w}} \tag{A4}$$

$$|HH'| = |GH'|\tan\psi_a = (x_H - B - \delta)\frac{n_w/n_a\sin\psi_w}{\sqrt{1 - n_w^2/n_a^2\sin^2\psi_w}} \tag{A5}$$

Substituting Eqs. A2 through A5 to Eq. A1, the equation for sin ψ_w can be obtained as in Equation 11, which can then be solved using Newton's method.

Calculation of cos ψ_1 and cos ψ_2

Given point P′(x', y', z'), and H(x_H, y_H, z_H), the coordinate of point P(x, y, z) on the inner surface of the sleeve can be expressed as

$$P\left(B,\, y' + \frac{(B - x')(y_H - y')}{d_s \cot \psi_w},\, z' + \frac{(B - x')(z_H - z')}{d_s \cot \psi_w}\right) \tag{A6}$$

The line PP′ can then be expressed as

$$PP' : \left\{1,\, \frac{y_H - y'}{d_s \cot \psi_w},\, \frac{z_H - z'}{d_s \cot \psi_w}\right\} \tag{A7}$$

The upper wing of the corrugated plate can be represented by

$$x' - z' \cot \alpha = 0 \tag{A8}$$

Let N_1 indicate the normal of the upper wing, the cosine of the angle between the normal of the upper wing and line PP′ can be obtained

$$\cos \psi_1 = \frac{|N_1 \cdot PP'|}{|N_1|\,|PP'|} = \frac{d_s \tan \alpha - (z_H - z') \tan \psi_w}{d_s} \cos \psi_w \cos \alpha \tag{A9}$$

The light ray from H on the surface of the lamp intercepts with the outer surface of the sleeve at point G. The coordinate of point G can be expressed as

$$G\left(B + \delta,\, y_H - \frac{(y_H - B - \delta)(y_H - y') \tan \psi_a}{d_s},\, z_H - \frac{(z_H - B - \delta)(z_H - z') \tan \psi_a}{d_s}\right) \tag{A10}$$

and the line GH can then be expressed as

$$GH : \left\{1,\, \frac{(y_H - y') \tan \psi_a}{d_s},\, \frac{(z_H - z') \tan \psi_a}{d_s}\right\} \tag{A11}$$

The surface of the lamp can be represented by

$$(x_H - B - C - \delta)^2 + y_H^2 = D^2/4 \tag{A12}$$

The normal of the lamp surface has the form of

$$N_2 : \{x_H - B - C - \delta,\, y_H,\, 0\} \tag{A13}$$

Therefore, the cosine of the angle between the normal of the lamp surface and the line GH can be obtained as

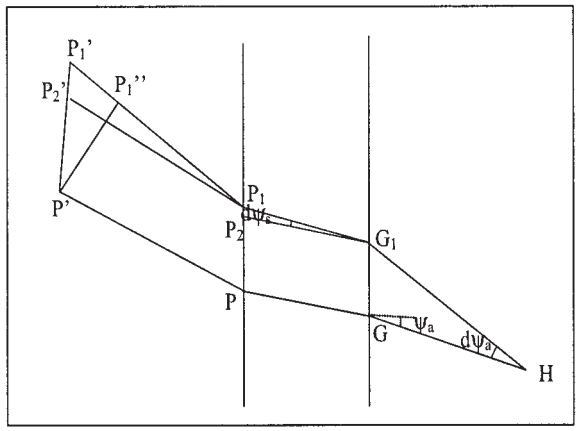

Figure A2. Area dS_w formed by the light rays from point H on the lamp.

$$\cos \psi_2 = \frac{|N_2 \cdot GH|}{|N_2|\,|GH|} = \frac{2 \cos \psi_a (x_H - B - C - \delta)}{D} + \frac{2 y_H \sin \psi_a (y_H - y')}{D d_s}. \tag{A14}$$

Calculation of $\mathbf{dS_w}$

In computing the incidence energy rate at the corrugated plate from the cylindrical lamp, it is necessary to get the area that is covered in the upper wing of the corrugated plate from the light rays at point H within the solid angle $\sin \psi_a d\psi_a d\theta$ of the cylindrical lamp. Figure A2 illustrates the two light rays from point H with the incidence angles being ψ_a and $\psi_a + d\psi_a$, respectively. Analyzing the geometric relations, the following equation holds

$$|P'P_1'| = |GG_1| + |P_1P_2| + |P_1'P_2'| = \left(\frac{x_H - B - \delta}{\cos^2 \psi_a} + \frac{\delta}{\cos^2 \psi_s} \frac{d\psi_s}{d\psi_a} + \frac{B - x'}{\cos^2 \psi_w} \frac{d\psi_w}{d\psi_a}\right) d\psi_a = \left(\frac{x_H - B - \delta}{\cos^2 \psi_a} + \frac{\delta}{\cos^2 \psi_s} \frac{n_a \cos \psi_a}{n_s \cos \psi_s} + \frac{B - x'}{\cos^2 \psi_w} \frac{n_a \cos \psi_a}{n_w \cos \psi_w}\right) d\psi_a \tag{A15}$$

If we define

$$d_r = \left(\frac{x_H - B - \delta}{\cos^2 \psi_a} + \frac{\delta}{\cos^2 \psi_s} \frac{n_a \cos \psi_a}{n_s \cos \psi_s} + \frac{B - x'}{\cos^2 \psi_w} \frac{n_a \cos \psi_a}{n_w \cos \psi_w}\right) \cos \psi_w \tag{A16}$$

the distance of $P'P_1''$ can be written as

$$|P'P_1''| = d_r d\psi_a \tag{A17}$$

Figure A3 illustrates the three-dimensional (3-D) diagram of the area covered by the light rays from point H within the solid

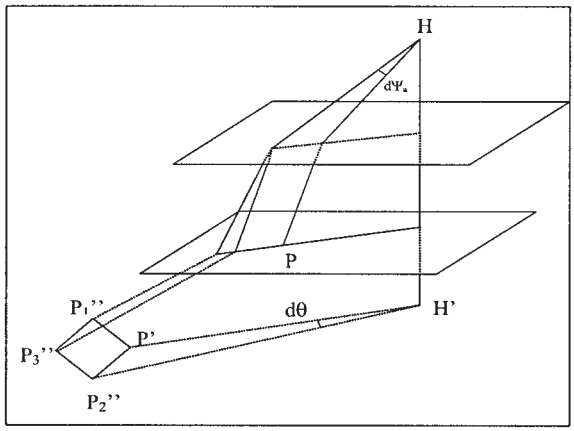

Figure A3. Area dS_w formed by the light rays from point H on the lamp.

angle sin $\psi_a d\psi_a d\theta$ of the cylindrical lamp. The area $P'P''_1P''_2P''_3$ is perpendicular to the light rays. It is easy to see that

$$|P'P''_2| = |P'H'|d\theta = \sqrt{(y' - y_H)^2 + (z' - z_H)^2}\, d\theta = d_s d\theta \tag{A18}$$

The area of $P'P''_1P''_2P''_3$ can be expressed as

$$S_{P'P''_1P''_2P''_3} = d_r d_s d\psi_a d\theta \tag{A19}$$

Therefore, the area in the plane of upper wing of the corrugated plate that is covered by the light rays at point H within the solid angle sin $\psi_a d\psi_a d\theta$ of the cylindrical lamp has the form as in Equation 19.

Manuscript received Aug. 30, 2004, and revision received Nov. 4, 2004.